Microscopic theory of electrodynamic response of diffuse jellium surfaces

Peter Gies
Institut für Theoretische Physik, Freie Universität Berlin, D-1000 Berlin 33, Federal Republic of Germany

Rolf R. Gerhardts
Max-Planck-Institut für Festkörperforschung, D-7000 Stuttgart 80, Federal Republic of Germany

Tsofar Maniv
Department of Chemistry, Technion—Israel Institute of Technology, 32 000 Haifa, Israel
(Received 13 June 1986)

A finite-slab mixed Fourier representation is used to study, within the random-phase approximation, the electromagnetic response of a jellium-metal film of arbitrary thickness, with a general form of the single-electron potential barrier defining the surface. Application is made to the calculation of various optical properties both for simple steplike potential barriers and the Lang-Kohn self-consistent potential. It is found that smooth potential barriers tend to support a localized collective excitation within the electronic charge-density tail at the surface, which is manifested by a dramatic enhancement of the optical power absorption. For thin films, finite-size oscillations are found in the surface response function below the plasma frequency, which are more pronounced for the steplike than for the Lang-Kohn potential well.

I. INTRODUCTION

The modern optical methods for the characterization of clean and adsorbate-covered metal surfaces, such as the different types of difference reflection spectroscopy, excitation of surface plasmons, ultraviolet photoemission, etc., cannot satisfactorily be described within the framework of classical Fresnel optics, which considers only transverse-wave solutions of Maxwell's equations. Incident light with a finite normal component of the electric field vector induces screening charges in the surface region, which extend typically some angstroms into the metal and produce a longitudinal contribution to the electromagnetic surface fields. This longitudinal electric field depends strongly on specific surface properties, for instance, the unperturbed electronic charge-density profile, and determines the surface-specific experimental results. An adequate theory should realistically describe both the optically induced charges, i.e., optical electron-hole pair or collective plasma excitations near the surface, and the effect of the detailed electronic surface structure on the optical response. Phenomenological generalizations of Fresnel optics have emphasized one or the other of these aspects, but a consistent treatment requires a microscopic theory of electromagnetic surface response.[1]

Microscopic approaches to metal optics, based on the jellium model for conduction electrons and on the random-phase approximation (RPA) for their response properties, have been presented by Feibelman,[2,3] by Maniv and Metiu[4–6] (MM), and by Gerhardts and Kempa[7] (GK). Feibelman used Maxwell's equations to calculate the linear response to the self-consistent electric field of electrons kept inside a jellium halfspace by the effective surface potential calculated by Lang and Kohn.[8] He considered an incident plane light wave and made extensive use of the fact that its vacuum wavelength is much larger than the typical spatial extent of optically induced charges ("long-wavelength limit"). Since he worked in real space and did not include bulk damping effects, a clever treatment of long-range field contributions owing to propagating plasma waves and to Friedel-type oscillations was necessary in the numerical calculations.

Maniv and Metiu avoided the restriction of long wavelengths and addressed the RPA response of a jellium slab to an arbitrary external electromagnetic field, including, for example, the field of an oscillating dipole near the surface.[9] Working in a mixed Fourier representation,[4] MM recognized that the simultaneous occurrence of long-range "bulk" fields and short-range "surface" fields leads to numerical problems which can be circumvented by a suitable renormalization of the dielectric response tensor.[4–6] In the renormalized version, only the short-range effects remain to be calculated numerically, whereas the long-range effects are treated analytically. Using the mixed Fourier representation of Maxwell's equations for a jellium halfspace, Gerhardts and Kempa[7] showed that, in the long-wavelength limit, longitudinal fields, which are of short range, decouple from the transverse long-range fields, and they obtained results equivalent to those of MM's renormalization procedure.

A shortcoming of the explicit calculations of both MM and GK is the use of the simple infinite-barrier model (IBM) for the effective potential. It is well known[10] that the IBM leads to a much steeper electron-density profile than the more realistic Lang-Kohn potential. As a consequence, some surface response properties calculated by GK,[7] e.g., the photoabsorption spectrum, show strong disagreement with Feibelman's results.[3]

The purpose of the present paper is to extend the mixed Fourier formalism to arbitrary one-dimensional potential

wells, so that a systematic investigation of the effect of the specific surface potential on several response properties becomes possible. The idea is simple: Since the electron density outside the metal decays rapidly both in the ground state and under illumination, one can introduce two auxiliary infinite potential barriers sufficiently far from the physical surfaces of the metal slab so that neither the electron density in the ground state nor the optical response properties are considerably affected. Then the mixed Fourier representation can be applied between the barriers, whereas we have vacuum fields outside. The selection of the barrier positions is admittedly somewhat arbitrary, but our computations have shown that, for photon frequencies ω of the order of the plasma frequency ω_p or smaller, the procedure is rather insensitive to the exact location of the auxiliary infinite barriers, provided that their distance from the jellium edge is larger than about 4 Å. In recent work on the static and low-frequency response of metal surfaces similar models have been used.[11–15]

The paper is organized as follows. In Sec. II we briefly recall some basic results of the IBM calculation by MM and indicate the modifications necessary to include smooth surface potentials. Especially, we summarize the important results for surface-sensitive quantities in the long-wavelength limit. In the Appendix we sketch the derivation of these results within the alternative approach in the spirit of GK, starting from Maxwell's equations for the slab geometry. This demonstrates the equivalence of the approaches.

In Sec. III the formal properties of the longitudinal dielectric matrix, such as sum rules, are discussed. In Sec. IV we present numerical results for different quantum-mechanical surface models and discuss their physical implications. A short summary and conclusions are given in Sec. V.

II. FORMAL RESULTS

A. Renormalization procedure

We consider an electron gas bounded by a one-dimensional potential well, as illustrated schematically in Fig. 1. Auxiliary potential barriers at $z=0$ and $z=L$ are introduced on both sides of the potential well, and the positively charged jellium background is situated between a and $L-a$. The distance a is chosen sufficiently large so that the final results are practically independent of a. For computational convenience, we assume inversion symmetry of the unperturbed system with respect to $z=\frac{1}{2}L$.

The general dielectric response tensor $\Pi_{\nu,\nu'}(\mathbf{K},z,z';\omega)$ of the bound electron system, as well as the bare (vacuum) photon propagator $D_{\nu}^{(0)}(\mathbf{K},z,z';\omega)$, can be expanded in the mixed Fourier representation[4] corresponding to a slab of thickness L, which is determined by the positions of the auxiliary barriers. The subscripts ν denote timelike ($\nu=0$) and spacelike ($\nu=1,2,3$) components, and $\mathbf{K}$ is the two-dimensional wave vector parallel to the slab, which has translational symmetry in the x-y plane. The resulting self-consistency equation for $\Pi_{\nu,\nu'}$ within the RPA is given by

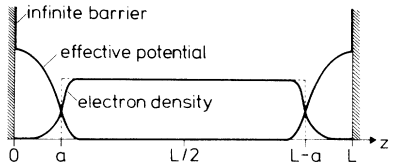

FIG. 1. Model system with a jellium slab of width $L-2a$, located symmetrically between two auxiliary infinite potential barriers. Electron density and effective potential are indicated.

$$\Pi_{\nu,\nu'}(k,k')=\Pi_{\nu,\nu'}^{(0)}(k,k') -2\pi^2 L\sum_{p,p',\mu}\Pi_{\nu,\mu}^{(0)}(k,p) \times D_{\mu}^{(0)}(p,p')\Pi_{\mu,\nu'}(p',k') , \quad (2.1)$$

where k,k' and p,p' all take values of the form $n\pi/L$ with n equal to odd (even) integers for a symmetric (antisymmetric) response.[4,10] The structure of this equation is identical to that of the corresponding equation in the IBM;[4] the only difference concerns the explicit form of the bare polarization tensor $\Pi_{\nu,\nu'}^{(0)}(\mathbf{K},k,k';\omega)$ which must be recalculated anew for each single-electron model potential.

The great advantage of using this representation is, however, that the bare photon propagator $D_{\mu}^{(0)}(p,p')$ is identical to that of the IBM calculation,[5,6] so that the renormalization scheme applied in the IBM calculations is applicable also in the present more general situation. Application of this renormalization procedure transforms Eq. (2.1) into

$$\sum_{p,\mu}\bar{\epsilon}_{k\nu,p\mu}\bar{\Pi}_{\mu,\nu'}(p,k')=\Pi_{\nu,\nu'}^{(0)}(k,k') , \quad (2.2)$$

where the renormalized dielectric tensor is defined by

$$\bar{\epsilon}_{k\nu,p\mu}=\delta_{k\nu,p\mu}+2\pi^2 L\,\Pi_{\nu,\mu}^{(0)}(k,p)D_{\mu}^{(0)}(p) , \quad (2.3)$$

and $D_{\mu}^{(0)}(p)$ is the diagonal part of the vacuum photon propagator $D_{\mu}^{(0)}(p,p')$. This renormalization eliminates from the self-consistency equation all the nonadditive long-wavelength contributions, which generate the reflected photon beam.[5,6] A formal solution for the renormalized response tensor $\bar{\Pi}_{\nu,\nu'}(k,k')$ in terms of the inverse dielectric matrix $\bar{\epsilon}^{-1}_{k\nu,k'\nu'}$ is given by

$$\bar{\Pi}_{\nu,\nu'}(k,k')=[2\pi^2 L D_{\nu'}^{(0)}(k')]^{-1}(\delta_{k\nu,k'\nu'}-\bar{\epsilon}^{-1}_{k\nu,k'\nu'}) . \quad (2.4)$$

In the long-wavelength limit, where the coupling between the transverse and the longitudinal components of the response tensor can be neglected,[7] the short-wavelength response function, which dominates the optical properties over a length scale of a few angstroms around the surface, is completely determined by the inverse of the density-density dielectric matrix $\bar{\epsilon}_{k0,k'0}$.[5,6] Furthermore, if the sources of the external electromagnetic fields are located outside the auxiliary infinite barriers as, for instance, in the case of an incident plane wave considered in the present paper, the individual components of $\bar{\epsilon}^{-1}_{k0,k'0}$ contain a surplus of information, and the short-

wavelength dielectric response is completely determined by the sum[5,6]

$$\bar{\epsilon}_l^{-1}(\mathbf{K},k;\omega)\equiv\sum_{k'}\bar{\epsilon}^{-1}_{k0,k'0}(\mathbf{K};\omega)\ . \tag{2.5}$$

This result can also be obtained from the evaluation of Maxwell's equations,[7] which yields as a simplified version of Eq. (2.2) (cf. also the Appendix)

$$\sum_{k'}\bar{\epsilon}_{k0,k'0}(\mathbf{K};\omega)\bar{\epsilon}_l^{-1}(\mathbf{K},k';\omega)=1\ . \tag{2.6}$$

B. Surface-sensitive observables

As we have already mentioned, the introduction of the auxiliary infinite barriers and the use of the corresponding mixed Fourier representation enable us to adopt all the formulas derived previously within the IBM for calculating various surface-sensitive observables, provided that the bare polarization $\Pi^{(0)}_{0,0}(\mathbf{K},k,k';\omega)$ is calculated for the actual effective potential sketched in Fig. 1. For example, the surface-sensitive component of the electric field [i.e., $E_z(z)$ for z inside the slab near the slab boundary] can be computed by using Eq. (V.6) of Ref. 6, that is,

$$E_z(z)=E_z^{\rm inc}[(1+r^{\rm odd}+r^{\rm even})e^{-ik_0z}+(r^{\rm odd}-r^{\rm even})e^{-ik_0(L-z)}+\Delta\bar{e}_z(z)]\ , \tag{2.7}$$

where $E_z^{\rm inc}$ is the z component of the incident field, $r^{\rm odd}$ ($r^{\rm even}$) is the odd (even) reflection coefficient defined in Eq. (IV.30) of Ref. 5, $k_0=(\omega/c)\cos\phi$ with ϕ the angle of incidence of the photon beam, and

$$\Delta\bar{e}_z(z)=\frac{4}{L}\sum_{\substack{k>0\\ \rm odd}}\frac{\sin(kz)}{k}[\bar{\epsilon}_l^{-1}(k)-1](1+e^{-ik_0L})(r^{\rm odd}+\tfrac{1}{2})+\frac{4}{L}\sum_{\substack{k>0\\ \rm even}}\frac{\sin(kz)}{k}[\bar{\epsilon}_l^{-1}(k)-1](1-e^{-ik_0L})(r^{\rm even}+\tfrac{1}{2})\ . \tag{2.8}$$

Here we have omitted the arguments $\mathbf{K}$ and ω of the effective inverse longitudinal dielectric function introduced by Eq. (2.5).[16]

Equations (2.7) and (2.8) are valid for any value of the slab thickness L and, therefore, can be used for very thin films and for a semi-infinite metal as well. In the limit $k_0L\to\infty$ (semi-infinite metal), the odd and even contributions to the reflection coefficient r become equal, $r^{\rm odd}=r^{\rm even}=\frac{1}{2}r$, and the sums in Eq. (2.8) can be replaced by integrals. Then, the singular terms $\exp(-ik_0L)$ in Eq. (2.8) cancel each other and

$$\Delta\bar{e}_z(z)=(r+1)\frac{4}{L}\sum_{\substack{k>0\\ \rm odd}}\frac{\sin(kz)}{k}[\bar{\epsilon}_l^{-1}(k)-1]\to(r+1)\frac{2}{\pi}\int_0^\infty dk\frac{\sin(kz)}{k}[\bar{\epsilon}_l^{-1}(k)-1]\ . \tag{2.9}$$

On the other hand, for a very thin film ($k_0L\ll1$), Eq. (2.8) reduces to

$$\Delta\bar{e}_z(z)\approx\frac{4}{L}\sum_{\substack{k>0\\ \rm odd}}\frac{\sin(kz)}{z}[\bar{\epsilon}_l^{-1}(k)-1](r+1)\ , \tag{2.10}$$

since in this limit $r\approx2r^{\rm odd}$. Note that formally the results for $\Delta\bar{e}_z(z)$ are the same both for a very thin film and a semi-infinite metal. The values of the reflection coefficients in the two limits, however, are quite different. For a semi-infinite metal, one can use, to a good approximation, the expression given by the classical Fresnel formula, while for a very thin film, one may use Eq. (IV.47) of Ref. 5, i.e.,

$$r\approx2r^{\rm odd}\approx(\tan\phi)^2U^{\rm odd}_{0,0}\ , \tag{2.11}$$

where

$$U^{\rm odd}_{0,0}\equiv i\frac{\omega}{c}(\cos\phi)\frac{4}{L}\sum_{\substack{k>0\\ \rm odd}}[\bar{\epsilon}_l^{-1}(k)-1]\frac{1}{k^2}\ . \tag{2.12}$$

In the Appendix we derive a formula which includes the effect of the transverse field, too. We can also give immediately an expression for the photoabsorption due to energy transfer processes through the longitudinal field by using Eq. (VI.5) of Ref. 5, that is,[16]

$$Y(\omega)\approx\frac{\omega}{c}(\sin\phi)(\tan\phi)\,|\,1+r\,|^2\frac{4}{L}\sum_{\substack{k>0\\ \rm odd}}{\rm Im}[-\bar{\epsilon}_l^{-1}(k)]/k^2\ . \tag{2.13}$$

Again this approximation is valid both for very thin films and for a semi-infinite metal. It should be noted, however, that only in the thin-film limit Eq. (2.13) yields a well-defined quantity. In the semi-infinite limit the sum in Eq. (2.13) develops a long-wavelength singularity, which should be treated carefully. To handle the long-wavelength contribution to the photoabsorption correctly, one should take into account also the transverse components of the electromagnetic field, which yield an effective cutoff of the long-wavelength singularity (cf. the Appendix).

III. DIELECTRIC MATRIX

A. Formal evaluation

It is clear now that the interesting longitudinal corrections to the classical Fresnel optics are determined by the effective inverse dielectric function $\bar{\epsilon}_l^{-1}(\mathbf{K},k';\omega)$, which is the solution of the set of linear equations (2.6). Thus, the key quantity to be computed is the kernel of this equation,

the density-density dielectric matrix $\bar{\epsilon}_{k0,k'0}(\mathbf{K};\omega)$. This can be done through the relation [cf. Eq. (2.3)]

$$\bar{\epsilon}_{k0,k'0}(\mathbf{K};\omega)\approx\delta_{k,k'}+2\pi^2 L\,\Pi^{(0)}_{0,0}(\mathbf{K},k,k';\omega)4\pi/(k')^2 , \quad (3.1)$$

once the density-density component of the bare polarization tensor is known. The latter will be calculated from the standard RPA formula appropriate for a system which is translational-invariant in the x-y directions:

$$\Pi^{(0)}_{0,0}(\mathbf{K},z,z';\omega)=\frac{e^2}{8\pi^4}\int d^2Q\sum_{n,n'}\frac{f(E_{n,\mathbf{Q}})-f(E_{n',\mathbf{Q}+\mathbf{K}})}{E_{n',\mathbf{Q}+\mathbf{K}}-E_{n,\mathbf{Q}}-\hbar\tilde{\omega}}\phi^*_n(z)\phi_{n'}(z)\phi_n(z')\phi^*_{n'}(z') . \quad (3.2)$$

Here f is the Fermi function, $\mathbf{K}$ and $\mathbf{Q}$ are wave vectors in the x-y plane, and $\tilde{\omega}\equiv\omega+i\gamma\,\mathrm{sgn}(\omega)$ is the complex photon frequency, the imaginary part of which is determined by the phenomenological damping constant γ.

A proper way to introduce γ without violation of the equation of continuity has been discussed in Ref. 4. The energies appearing in Eq. (3.2) are of the form

$$E_{n,\mathbf{Q}}=\varepsilon_n+\hbar^2(Q_x^2+Q_y^2)/(2m_0) , \quad (3.3)$$

with ε_n and $\phi_n(z)$ the energy eigenvalues and eigenfunctions of the one-dimensional Schrödinger equation corresponding to the model potential under study, which includes, in addition to the actual surface potential, the two auxiliary infinite barriers. The free-electron mass is denoted by m_0.

Introducing the dimensionless Fourier coefficients

$$W_k^{n,n'}=2\int_0^L dz\cos(kz)\phi^*_n(z)\phi_{n'}(z) \quad (3.4)$$

with $k=m\pi/L$ and m integer, we obtain for the double cosine transform of Eq. (3.2) in the zero-temperature limit, in which the two-dimensional $\mathbf{Q}$ integral of Eq. (3.2) can be done analytically,[6]

$$\Pi^{(0)}_{0,0}(\mathbf{K},k,k';\omega)=\frac{e^2}{2(\pi L)^2}\sum_{n,n'}W_k^{n,n'}W_{k'}^{n',n}\mathscr{H}(\mathbf{K},n,n';\omega) , \quad (3.5)$$

where

$$\mathscr{H}(\mathbf{K},n,n';\omega)=\frac{m_0}{2\pi\hbar^2}\frac{k_F}{K}\left[1-\frac{\varepsilon_n}{\varepsilon_F}\right]^{1/2}\Theta(1-\varepsilon_n/\varepsilon_F)\times[F(u_+)+F(u_-)] , \quad (3.6)$$

with $\Theta(x)$ the unit step function, ε_F the Fermi energy, $k_F=(2m_0\varepsilon_F)^{1/2}/\hbar$ the Fermi wave number, $K=|\mathbf{K}|$,

$$u_\pm=\frac{1}{2}\frac{(\varepsilon_n-\varepsilon_{n'}\pm\hbar\tilde{\omega})/\varepsilon_F-K^2/k_F^2}{(K/k_F)(1-\varepsilon_n/\varepsilon_F)^{1/2}} , \quad (3.7)$$

and

$$F(u)=\frac{1}{\pi}\int_{-1}^{1}dx\frac{(1-x^2)^{1/2}}{x-u}=u\left[\left[1-\frac{1}{u^2}\right]^{1/2}-1\right] . \quad (3.8)$$

The function $F(u)$ is analytic in the complex u plane with a branch cut at $-1<u<1$. In the long-wavelength limit [$K\to 0$, $F(u)\approx -1/2u$] we need only

$$\mathscr{H}(0,n,n';\omega)=-\frac{m_0}{\pi\hbar^2}\Theta\left[1-\frac{\varepsilon_n}{\varepsilon_F}\right]\frac{(\varepsilon_F-\varepsilon_n)(\varepsilon_n-\varepsilon_{n'})}{(\varepsilon_n-\varepsilon_{n'})^2-(\hbar\tilde{\omega})^2} . \quad (3.9)$$

Together with Eq. (3.5) this yields for the dielectric matrix [cf. Eq. (3.1)] in the long-wavelength limit

$$\bar{\epsilon}_{k0,k'0}(0;\omega)=\delta_{kk'}-\frac{4}{a_0L(k')^2}\sum_{\substack{n,n'\\ \varepsilon_n<\varepsilon_F}}\frac{(\varepsilon_F-\varepsilon_n)(\varepsilon_n-\varepsilon_{n'})}{(\varepsilon_n-\varepsilon_{n'})^2-(\hbar\tilde{\omega})^2}\times W_k^{n,n'}W_{k'}^{n',n} , \quad (3.10)$$

where $a_0=\hbar^2/(e^2m_0)$ is the Bohr radius.

B. Symmetry and sum rules

One of the advantages of having two infinite barriers included in the single-electron potential is that the wave functions $\phi_n(z)$ as well as any response functions of the system strictly vanish at $z=0$ and $z=L$. This implies sum rules for the Fourier coefficients of cosine transforms. For instance, the bare polarization matrix $\Pi^{(0)}_{0,0}(\mathbf{K},k,k';\omega)$ (as well as the full one $\bar{\Pi}_{0,0}$) satisfies the exact sum rules

$$\sum_k\Pi^{(0)}_{0,0}(k,k')=\sum_{k'}\Pi^{(0)}_{0,0}(k,k')=0 , \quad (3.11)$$

and the coefficients defined in Eq. (3.4) satisfy

$$\sum_k W_k^{n,n'}=0 . \quad (3.12)$$

(If one restricts the sums to $k\geq 0$, the $k=0$ terms should be taken with a factor $\frac{1}{2}$.) For the numerical calculation of these coefficients, a sine expansion of the wave functions with Fourier coefficients

$$c_n(k)=(2/L)^{1/2}\int_0^L dz\sin(kz)\phi_n(z) \quad (3.13)$$

is convenient. We will consider only such models for the single-electron potenial which are symmetric with respect to the center $z=\frac{1}{2}L$ of the slab. Then the wave functions have definite parity; they are real, even or odd functions of the variable $z-\frac{1}{2}L$. The coefficients $c_n(k)$ ($n=0,1,2,\ldots$) vanish if $\phi_n(z)$ and $\sin kz$ have different parity, i.e., $c_n(k)=0$ if $\phi_n(z)$ is an even (odd) function of $z-\frac{1}{2}L$ and if $m=Lk/\pi$ is an even (odd) integer. Simi-

larly, the coefficients $W_k^{n,n'}$ defined in Eq. (3.4) vanish if the product $\phi_n(z)\phi_{n'}(z)$ and the function $\cos kz$ (or, equivalently, the integer number kL/π) have different parity. As a consequence, only k and k' values of the same parity, either both odd or both even multiples of π/L, are coupled by the dielectric matrix, Eqs. (3.1) and (3.10). As emphasized in Sec. II, for very thin films and for semi-infinite metals, only the odd response modes need to be considered explicitly. We take advantage of this simplification in our numerical computations.

Inserting the sine expansion of the wave functions into Eq. (3.4), one obtains (for $pL/\pi=0,1,2,\ldots$)

$$W_p^{n,n'}=\sum_{k,k'} c_n(k)c_{n'}(k')(\delta_{k'-k,p}+\delta_{k-k',p}-\delta_{k+k',p}) , \tag{3.14}$$

where the sum is over all values $kL/\pi=1,2,\ldots$ and $k'L/\pi=1,2,\ldots$, and the sum rule (3.12) is evident. In order to satisfy the sum rules (3.11) and (3.12) exactly also in the numerical calculations, where only a finite number of coefficients is available, we proceed as follows. First, we choose an upper bound P larger than the maximum values of k and k' we want to keep in the dielectric matrix (3.10). Then we compute $c_n(k)$ and $c_{n'}(k')$ by numerical integration according to Eq. (3.13) for all values of $k\le P$ and $k'\le P$. Finally, we compute for all values $p\le P$ the coefficients $W_p^{n,n'}$ according to Eq. (3.14); however, with the additional restriction $k+k'\le P$.

An advantage of our approach is that the coefficients $W_k^{n,n'}$ and the energy eigenvalues ε_n in Eq. (3.10) must be calculated only once, even if one wants to calculate the dielectric matrix for different frequencies ω. Green's-function methods,[2] on the other hand, require a new numerical integration of Schrödinger's equation for each value of ω. The n' sum in Eq. (3.10) converges reasonably quickly and is truncated at a sufficiently high energy $\varepsilon_{n'}$. Note that a truncation is not necessary for the simple IBM, where Eq. (3.13) reduces to $c_n(k)=\delta_{n,k}$, so that no sum is left in Eq. (3.14) and the n' sum in Eq. (3.10) becomes trivial.

IV. APPLICATION AND NUMERICAL RESULTS

It was suspected that the electron density profile at a metal surface strongly affects the optical response properties.[7,17,18] In this section we will present results for three different surface-model potentials: the self-consistent effective potential calculated by Lang and Kohn,[8] which has been used in Feibelman's response calculation;[3] the simple IBM employed by MM and by GK; and further a so-called finite-barrier model (FBM) with the surface potential represented by a single step. Results on strongly charged jellium surfaces, for which the electron density is altered by the applied static electric field, have been reported elsewhere.[19]

In the long-wavelength limit, which will be considered exclusively in this section, and for sufficiently large film thickness, numerous response properties can be expressed conveniently in terms of the surface response functions $d_\perp(\omega),d_\parallel(\omega)$ first introduced by Feibelman,[3,20] in order to describe the electromagnetic response of a jellium halfspace. They are defined as

$$d_\perp=\int dz[E_z(z)-E_z^{\rm cl}(z)]/[E_z^{\rm cl}({\rm out})-E_z^{\rm cl}({\rm in})] , \tag{4.1}$$

$$d_\parallel=\int dz[D_x(z)-D_x^{\rm cl}(z)]/[D_x^{\rm cl}({\rm out})-D_x^{\rm cl}({\rm in})] . \tag{4.2}$$

Here, the superscript cl refers to the classical transverse field, which varies discontinuously at the surface, out (in) indicates the region outside (inside) the metal, and the integrals extend over the surface region, where the actual fields $E_z(z),D_x(z)$ deviate from the classical fields. The film thickness or, alternatively, the damping constant γ, shall be so large, that in the center region the actual fields are equal to the classical fields. As shown in the Appendix, we determine the classical fields by specifying a transverse dielectric constant ϵ_t in the slab region $0<z<L$. Then, from the RPA result for the dielectric tensor,

$$\epsilon_{xx}(z,z')=\delta(z-z')[1+(\epsilon_t-1)n(z)/n_+] ,$$

[with $n(z)$ the electron density and n_+ the jellium density] one obtains, for the left-hand surface, $d_\parallel=a$, i.e., the location of the jellium edge.[1,3,7,17] The integrand in Eq. (4.1) can be regarded as a normalized longitudinal field,[3,7] which can be written in the form (cf. the Appendix)

$$-\xi(z)=(1-1/\epsilon_t)^{-1}E_z^l(z)/D_z(0) , \tag{4.3}$$

with the limiting values $\xi(0)=-1$ and $\xi(L/2)\approx 0$. Introducing the optically induced charge density ρ, which satisfies the equation $4\pi\rho=\nabla\cdot\mathbf{E}\approx dE_z^l/dz$, we can write Eq. (4.1) in the form

$$d_\perp=\int_0^{L/2} dz\, z\rho(z)\Big/\int_0^{L/2} dz\,\rho(z)\equiv\int_0^{L/2} dz\, z\bar{\rho}(z) . \tag{4.4}$$

Employing Eq. (2.10), we then obtain

$$d_\perp=\left[1-\frac{1}{\epsilon_t}\right]^{-1}\frac{4}{L}\sum_{\substack{k>0\\ \text{odd}}}\frac{1}{k^2}\left[\bar{\epsilon}_l^{-1}(k)-\frac{1}{\epsilon_t}\right] , \tag{4.5}$$

with the last term, $1/\epsilon_t$, taken instead of 1 in order to avoid the long-wavelength singularity mentioned at the end of Sec. II (cf. the discussion in the Appendix).

Results for the frequency dependence of $d_\perp$, calculated from Eq. (4.5) for three selected model potentials, are shown in Fig. 2. The film is chosen thick enough to ensure that, for the actual damping parameter, the longitudinal field becomes small near $z=\frac{1}{2}L$ but, on the other hand, thin enough to sustain odd response modes only. Obviously, the results for the three models are dramatically different. The real part of $d_\perp-d_\parallel$ which, according to Eq. (4.4), can be regarded as the center of gravity of the induced charge density, takes negative values for the Lang-Kohn and the FBM potential, if the frequency is low. That means the center of gravity of the induced charge density lies outside the jellium for these two models, whereas for the IBM, $\mathrm{Re}(d_\perp-d_\parallel)$ is positive, i.e., inside the jellium, for all frequencies below the plasma frequency ω_p. Also $\mathrm{Im}(d_\perp-d_\parallel)=\mathrm{Im}d_\perp$, which is closely related to the longitudinal-wave share of the photoabsorption coefficient [cf. Eq. (2.13)]

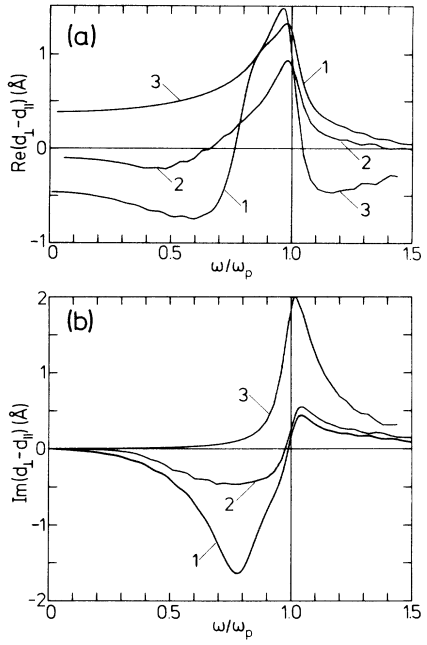

FIG. 2. (a) Real and (b) imaginary part of the surface response function $d_\perp - d_{||}$ for the Lang-Kohn potential (1), the FBM (2), and the IBM (3). The electron density is given by the Wigner-Seitz radius $r_s = (\frac{1}{3}4\pi n_+ a_0^3)^{-1/3} = 3$; further parameters are $L = 70$ Å, $a = 5$ Å for curves (1); $L = 60$ Å, $a = 5.3$ Å for curves (2); and $L = 60$ Å, $a = (3\pi^2/2)^{1/3} r_s a_0/4 \approx 0.97$ Å for curves (3); the damping constant is equal to $\gamma = 0.05\omega_p$ [$\omega_p = (4\pi n_+ e^2/m_0)^{1/2}$]. The barrier height in the FBM is twice the Fermi energy.

$$Y = \frac{\omega}{c}(\sin\phi)(\tan\phi)\,|\,1+r\,|^2 \mathrm{Im}\left[\left[\frac{1}{\epsilon_t}-1\right]d_\perp\right], \qquad (4.6)$$

turns out to be completely different for the three models. For the Lang-Kohn potential, $\mathrm{Im}d_\perp(\omega)$ exhibits a pronounced negative peak near $\omega = 0.8\omega_p$. As a consequence, the power absorption is, for this frequency range, dominated by the longitudinal field. Only immediately below

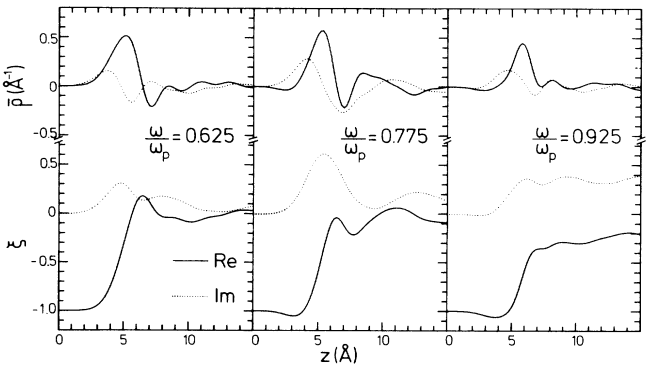

FIG. 3. Normalized longitudinal field $\xi(z)$ [cf. Eq. (4.3)] and normalized induced charge density $\bar{\rho}(z)$ for the Lang-Kohn potential at different values of the frequency ω. [Same parameters as in Fig. 2, curves (1).]

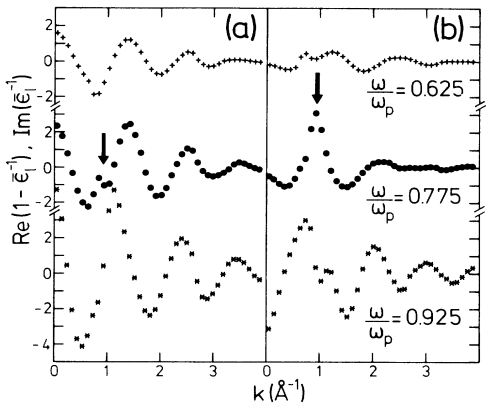

FIG. 4. Wave-vector dependence of the effective inverse longitudinal dielectric function, (a) $\mathrm{Re}(1-\bar{\epsilon}_l^{-1})$ and (b) $\mathrm{Im}\bar{\epsilon}_l^{-1}$, for different frequencies ω. A resonancelike structure at $k \approx 0.9$ Å^{-1}, marked by the arrows, emerges near $\omega = 0.775\omega_p$. The parameters are the same as for the Lang-Kohn potential in Fig. 2.

(and above) the plasma frequency, where the field penetrates far into the metal, does the damping due to the transverse field, described by the parameter γ, become important and lead to positive values of $\mathrm{Im}d_\perp(\omega)$. In the FBM, the peak structure below ω_p is smeared out, whereas the result for $\mathrm{Im}d_\perp(\omega)$ in the IBM is positive in the whole frequency region, and the damping is dominated by the transverse field. For the smooth Lang-Kohn potential, a peculiar S-like shape of $\mathrm{Re}(d_\perp - d_{||})$ emerges near the frequency where $-\mathrm{Im}d_\perp$ becomes maximum. This pole structure, which has first been calculated by Feibelman[3] for the semi-infinite system, has been attributed to a resonant plasmon excitation in the low-density region of the metal surface.[1,18,21,22] In the IBM the surface profile is far too steep to sustain such an excitation. The result for the FBM, which has a surface profile much steeper than the Lang-Kohn profile, but more diffuse than the IBM profile, is intermediate between these extreme cases. Of course, there is noticeable absorption due to optical electron-hole pair excitations near the surface, but no poletype structure emerges, which would indicate a resonant excitation.

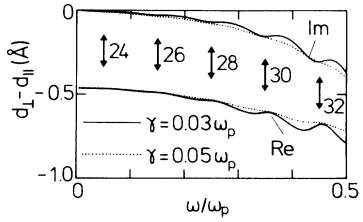

FIG. 5. Surface response function $d_\perp - d_{||}$ for the Lang-Kohn potential (parameters are the same as in Fig. 2). The solid curve is calculated with a reduced damping parameter γ, which is reflected in the more pronounced finite-size oscillations. The arrows mark the resonance frequencies (cf. the discussion in the text).

In order to shed some light on the poletype structure mentioned above, we calculated for the Lang-Kohn model the surface-sensitive part ξ of the induced electric field and the induced charge density ρ [cf. Eqs. (4.3),(4.4)]. In Fig. 3, results for frequencies $\omega/\omega_p=0.625$, 0.775, and 0.925 are presented. Pronounced structures in the field ξ are obtained for $\omega/\omega_p \sim 0.7$ to 0.8, and the induced charge density resembles a dipole layer, as is expected for the resonant excitation.[1,18,21,22] The effective inverse longitudinal dielectric function $\bar{\epsilon}_l^{-1}(k)$ itself, shown in Figure 4 for the same frequencies, exhibits a resonancelike structure at $\omega/\omega_p \approx 0.775$, $k \approx 0.9$ Å^{-1} as well. This structure, marked by the arrows in Fig. 4, vanishes rapidly if the frequency is changed. It is very similar to structures[6] due to plasmon excitations at frequencies above ω_p.

Finally, in Fig. 5 we examine the effect of the damping parameter γ on the surface response function $d_\perp$, calculated for the Lang-Kohn model. For the reduced damping, $\gamma=0.03\omega_p$, finite-size effects become visible, which are due to resonances in the dielectric function $\bar{\epsilon}_{k0,k'0}(0;\omega)$ [cf. Eq. (3.10)]. The finite-size effects occur because the single-electron energy levels, which are broadened by the damping, do not overlap completely in the potential well. The resonance condition for the frequency ω can be written as

$$\hbar\omega=\varepsilon_{n'}-\varepsilon_n \quad (n'=n+1,n+3,n+5,\ldots)\ , \tag{4.7}$$

with ε_n the energy of the highest occupied wave function. For the example under discussion, the number of occupied wave functions is given by $n=23$, and the first resonances occur at $n'=24$, 26, 28, 30, and 32, as indicated by the arrows in Fig. 5. Only odd response modes are considered here; therefore, $n+n'$ must be an odd integer. In the FBM, the finite-size effects are present as well, whereas in the simple IBM, they are completely absent due to the peculiar features of the coefficients $W_k^{n,n'}$ discussed at the end of Sec. III. It should be noted here that, if the value of the damping γ is so small that the artificial discrete nature of the spectrum above the vacuum edge becomes evident, the results at high frequencies are distorted by artificial finite-size effects due to the auxiliary infinite barriers.

Experimentally, finite-size oscillations should be seen, e.g., in the power absorption below the plasma frequency [cf. Eq. (4.6)], provided that the damping constant γ and the thickness of the metal film are sufficiently small. We want to stress that, apart from the finite-size effect, our result for the surface response function $d_\perp$, obtained for a jellium film, closely resembles the corresponding result of Feibelman for the semi-infinite case.

V. SUMMARY

We have applied the mixed Fourier formalism, previously employed by Maniv and Metiu and by Gerhardts and Kempa to discuss surface response properties in the framework of the oversimplified IBM, to the general case of an arbitrarily shaped surface-barrier potential. A finite jellium slab model was used, and auxiliary infinite potential barriers were situated sufficiently far away from the surfaces, so that the electron distribution in the ground state, as well as in the optically excited states, is practically independent of the actual position of the auxiliary barriers. Our method has several advantages over a direct real-space approach. For instance, cosine Fourier expansions yield exact sum rules, which can be employed to check numerical results. The Fourier coefficients of the density fluctuations have to be calculated from the numerically determined wave functions only once for all frequencies.

Our calculations for thin jellium films with the surface-barrier potential of Lang and Kohn have shown that the surface response function $d_\perp(\omega)$, calculated by Feibelman[3] for the semi-infinite system, can closely be reproduced already with films of about 60 Å thickness. Finite-size oscillations in the frequency dependence of $d_\perp(\omega)$ can be removed by choosing a sufficiently large phenomenological damping parameter γ, which leaves the overall structure of $d_\perp(\omega)$ nearly unchanged.

Different surface-model potentials yield a completely different behavior of the surface response function $d_\perp(\omega)$, which results in a dramatic increase of the optical power absorption, provided that the low-density tail of the electron distribution at the surface leaks out sufficiently far. This confirms previous results for the Lang-Kohn model[3] and for the IBM,[7] which could not be easily compared, since they were obtained with different approaches. Moreover, our calculations of the optically induced electric field and charge density support the assertion[1,7,18,21,22] that the enhanced photoabsorption obtained for the Lang-Kohn potential, which is in good agreement with the experimental photoyield spectrum of aluminum,[3,23] is due to a collective excitation mode, which is localized in the low-density tail of the electronic charge-density profile.

Finally, our calculations predict, that the optical spectra of very thin metal films (~ 100 Å) can show finite-size oscillations below the plasma frequency. Experimental investigations of this effect would be valuable.

ACKNOWLEDGMENT

Financial support by the Deutsche Forschungsgemeinschaft (Bonn, Federal Republic of Germany) through Sonderforschungsbereich 6 is gratefully acknowledged.

APPENDIX: MIXED FOURIER TRANSFORMATION OF MAXWELL'S EQUATIONS

We consider Maxwell's wave equation

$$\nabla(\nabla\cdot\mathbf{E})-\nabla^2\mathbf{E}=(\omega/c)^2\mathbf{D} \tag{A1}$$

for fields of the form

$$\mathbf{E}(\mathbf{r},t)=\mathbf{E}(z)\exp[i(q_x x-\omega t)]$$

in the slab geometry and assume local isotropic dielectric constants ϵ_a and ϵ_b for $z<0$ and for $z>L$ outside the slab, respectively. We assume incident p-polarized light with wave vector $(q_x,0,p_a)=(\epsilon_a)^{1/2}(\omega/c)(\sin\alpha,0,\cos\alpha)$ (here we choose the direction of incidence as in Ref. 7, i.e., opposite to that of Sec. II) so that $E_y\equiv 0$ and

$$\begin{aligned} E_x(z)&=-E_a(\cos\alpha)(e^{ip_a z}-re^{-ip_a z})\ , \\ E_z(z)&=E_a(\sin\alpha)(e^{ip_a z}+re^{-ip_a z})\ , \end{aligned} \tag{A2}$$

in $z<0$, whereas the transmitted beam in $z>L$ has the wave vector $(q_x,0,p_b)=(\epsilon_b)^{1/2}(\omega/c)(\sin\beta,0,\cos\beta)$ and

$$E_x(z)=-E_b(\cos\beta)e^{ip_bz}\ ,$$
$$E_z(z)=-(\tan\beta)E_x(z)\ . \tag{A3}$$

For $0<z<L$ inside the slab the x components (z components) of the electric field $\mathbf{E}(z)$ and the displacement $\mathbf{D}(z)$ are expanded in a cosine (sine) Fourier series according to

$$E_\mu(z)=\frac{1}{L}\sum_k \mathscr{E}_\mu(k)e^{ikz}\quad (Lk/\pi=0,\pm1,\pm2,\ldots)\ , \tag{A4}$$

with $\mathscr{E}_x(-k)=\mathscr{E}_x(k)$ and $\mathscr{E}_z(-k)=-\mathscr{E}_z(k)$ and similarly for $\mathscr{D}_\mu(k)$. Taking the cosine (sine) transform of the x (z) component of Eq. (A1) and introducing "longitudinal" ($\mathscr{E}_l,\mathscr{D}_l$) and "transverse" ($\mathscr{E}_t,\mathscr{D}_t$) field components[7] which are parallel and perpendicular to the vectors $\mathbf{q}=(q_x,0,k)$, respectively, we obtain Maxwell's equations in form

$$-\mathscr{D}_l(\mathbf{q})=\frac{i}{q}[D_z(0)-e^{ikL}D_z(L)]\ , \tag{A5a}$$
$$(c/\omega)^2q^2\mathscr{E}_t(\mathbf{q})-\mathscr{D}_t(\mathbf{q})=(k/q_x)\mathscr{D}_l(\mathbf{q})\ . \tag{A5b}$$

The response properties of the metal slab are described by constitutive equations of the form

$$\mathscr{D}_i(\mathbf{q})=\sum_{j=t,l}\sum_{k'}\epsilon_{ij}(q_x,k,k';\omega)\mathscr{E}_j(\mathbf{q}'),\quad i=t,l\ . \tag{A6}$$

In the long-wavelength limit the following approximation is appropriate:[7] neglect the coupling between longitudinal and transverse field components, $\epsilon_{tl}=\epsilon_{lt}=0$, replace ϵ_{tt} by the local Drude dielectric constant $\epsilon_t=1-\omega_p^2/[\omega(\omega+i\gamma)]$ of the bulk metal, and take the limit $q_x\to0$ in ϵ_{ll}. The component ϵ_{ll} of the dielectric tensor may either be calculated from the current-current correlation formula for the conductivity tensor[7] or from the density-density response function. (The equivalence follows from the generalized f-sum rule and the equation of continuity.[24])

Introducing effective dielectric functions

$$\bar\epsilon_j(\mathbf{q})=\mathscr{D}_j(\mathbf{q})/\mathscr{E}_j(\mathbf{q}),\quad j=t,l\ , \tag{A7}$$

we may write the nontrivial part of Eq. (A6) in the long-wavelength limit as

$$\sum_{k'}\frac{q}{q'}\epsilon_{ll}(q_x,k,k';\omega)\bar\epsilon_l^{-1}(\mathbf{q}')=1\ , \tag{A8}$$

which is just Eq. (2.6) with

$$\bar\epsilon_{k0,k'0}(\mathbf{K};\omega)=(q/q')\epsilon_{ll}(q_x,k,k';\omega)\ .$$

Here we took advantage of the decoupling of odd and even response modes.

From Eqs. (A4), (A5), and (A7) one obtains for the electric field in the slab

$$E_\mu(z)=f_\mu(z)D_z(0)+\eta_\mu f_\mu(L-z)D_z(L)\ , \tag{A9}$$

where $\eta_x=-1$, $\eta_z=+1$, and

$$f_\mu(z)=-\frac{i}{L}\sum_k\frac{e^{ikz}}{q^2}\left[\frac{kt_\mu}{c^2q^2/\omega^2-\bar\epsilon_t(\mathbf{q})}+\frac{q_\mu}{\bar\epsilon_l(\mathbf{q})}\right]\ , \tag{A10}$$

with $q_z=k$, $t_x=-k/q_x$, and $t_z=1$ [note that $\bar\epsilon_j(\mathbf{q})$ is an even function of k]. The constants r, E_b, $D_z(0)$, and $D_z(L)$ in Eqs. (A2), (A3), and (A9) are determined by the standard matching conditions (E_x and D_z continuous at $z=0$ and $z=L$). It is important to note that, for reasonable assumptions on the asymptotic behavior of the $\bar\epsilon_j(\mathbf{q})$ ($\bar\epsilon_t/q^2\to0$, $\bar\epsilon_l\to1$ for $k\to\infty$), the sine series (A10) for $f_z(z)$ is not absolutely convergent, and $f_z(0^+)\neq0$. The same is true for the longitudinal displacement field given by Eq. (A5a), which is easily evaluated as

$$D_\mu^l(z)=\frac{1}{L}\sum_k\frac{q_\mu}{q}\mathscr{D}_l(\mathbf{q})e^{ikz}$$
$$=g_\mu(z)D_z(0)+\eta_\mu g_\mu(L-z)D_z(L)\ , \tag{A11}$$

with

$$g_x(z)=-i\cosh[q_x(L-z)]/\sinh(q_xL)\ , \tag{A12a}$$
$$g_z(z)=\sinh[q_x(L-z)]/\sinh(q_xL)\ , \tag{A12b}$$

so that $D_z^l(0^+)=D_z(0)$, $D_z^l(L^-)=D_z(L)$, and $\nabla\cdot\mathbf{D}^l=0$ inside the slab. We find, that $f_z(0^+)=1/\bar\epsilon_l(q\to\infty)$, $f_z(L^-)=0$, and consequently, $E_z(0^+)=D_z(0)/\bar\epsilon_l(\infty)$, $E_z(L^-)=D_z(L)/\bar\epsilon_l(\infty)$. If we assume $\bar\epsilon_l(\infty)=1$ and vacuum outside the slab, $\epsilon_a=\epsilon_b=1$, we obtain both D_z and E_z continuous at $z=0$ and $z=L$, as it should be.[7] For the induced charged density we obtain from $4\pi\rho(\mathbf{r},t)=\nabla\cdot\mathbf{E}=\nabla\cdot(\mathbf{E}-\mathbf{D}^l)$ the cosine expansion

$$\rho(z)=h(z)D_z(0)-h(L-z)D_z(L)\ , \tag{A13}$$

with

$$h(z)=(4\pi L)^{-1}\sum_k\exp(ikz)[\bar\epsilon_l^{-1}(\mathbf{q})-1]\ , \tag{A14}$$

where we assumed $\bar\epsilon_l(\infty)=1$. For $D_z(0)\neq D_z(L)$, the vanishing of $\rho(z)$ near the infinite potential barriers implies $h(0^+)=h(L^-)=0$, i.e., two sum rules:

$$\sum_k[1-1/\bar\epsilon_l(\mathbf{q})]=0 \tag{A15}$$

must hold for the sum over the even and the odd values of kL/π separately. For $D_z(0)\approx D_z(L)$ (thin film) only the odd-integer sum rule survives. The limits of a very thin film and of a semi-infinite metal can easily be computed from Eq. (A10). First we consider the reflection coefficient r defined by Eq. (A2), which, owing to the matching condition at $z=0$, is given by

$$r=[1+\epsilon_a(\tan\alpha)Q_0]/[1-\epsilon_a(\tan\alpha)Q_0]\ , \tag{A16}$$

with [cf. Eq. (A9)]

$$Q_0\equiv E_x(0)/D_z(0)=f_x(0)-f_x(L)D_z(L)/D_z(0)\ . \tag{A17}$$

The matching condition at $z=L$ yields

$$D_z(L)/D_z(0)=f_x(L)/[f_x(0)-(\cot\beta)/\epsilon_b]\ . \tag{A18}$$

Now we separate even and odd contributions to $f_x(0)$, defining

$$2f_x^{\text{even}}=f_x(0)+f_x(L),\quad 2f_x^{\text{odd}}=f_x(0)-f_x(L)\ . \tag{A19}$$

For a very thin film, $\omega L/c \ll 1$, f_x^{even} is dominated by the large $k=0$ term [see Eq. (A10)]

$$f_x^{\text{even}}=1/[iq_xL\bar{\epsilon}_l(0)]+O(\omega L/c)\ , \tag{A20}$$

whereas, to leading order in $\omega L/c$,

$$2f_x^{\text{odd}}=\frac{i}{2}\frac{\omega^2}{c^2}\frac{L}{q_x}-\frac{4iq_x}{L}\sum_{\substack{k>0\\ \text{odd}}}\frac{1}{k^2\bar{\epsilon}_l(k)}\ . \tag{A21}$$

Then $f_x^{\text{odd}}/f_x^{\text{even}}\sim(q_xL)^2\ll 1$, and Eq. (A18) reduces to

$$D_z(L)/D_z(0)=1+ip_bL\bar{\epsilon}_l(0)/\epsilon_b\ , \tag{A22}$$

whereas Eqs. (A17) and (A18) yield

$$\begin{aligned}Q_0&=-\frac{1}{\epsilon_b}(\cot\beta)[1+(\cot\beta)/(\epsilon_b f_x^{\text{even}})-4\epsilon_b(\tan\beta)f_x^{\text{odd}}]\\&=-\frac{\cot\beta}{\epsilon_b}\left[1+ip_bL\left[\frac{\bar{\epsilon}_l(0)}{\epsilon_b}-1\right]\right.\\&\qquad\left.+i\epsilon_b\frac{8q_x^2}{p_bL}\sum_{\substack{k>0\\ \text{odd}}}\frac{1}{k^2}\left[\frac{1}{\bar{\epsilon}_l(k)}-\frac{1}{\epsilon_b}\right]\right]\ .\end{aligned} \tag{A23}$$

This result reduces to that obtained from local Fresnel optics for reflection from a thin surface layer of width L and dielectric constant ϵ_s on top of a dielectric halfspace with ϵ_b, if one replaces $\bar{\epsilon}_l(k)$ with ϵ_s. Note that the reflection amplitude r, Eq. (A16), is directly proportional to the thickness L of the slab, if the dielectric on both sides is the same, $\epsilon_b=\epsilon_a$, $\cos\beta=\cos\alpha$. For $\epsilon_b=\epsilon_a=1$ and $\alpha=\beta=\phi$, one obtains

$$\begin{aligned}r\approx-\frac{i}{2}\frac{\omega}{c}(\cos\phi)\Bigg[&L[\bar{\epsilon}_l(0)-1]\\&+\frac{8}{L}(\tan^2\phi)\sum_{\substack{k>0\\ \text{odd}}}\frac{1}{k^2}\left[\frac{1}{\bar{\epsilon}_l(k)}-1\right]\Bigg]\ ,\end{aligned} \tag{A24}$$

which is in agreement with Eq. (2.11); however, it includes also the contribution of the long-wavelength transverse field described by $\bar{\epsilon}_l(0)\equiv\bar{\epsilon}_t(0)$. For a semi-infinite metal, on the other hand, the k sums converge to k integrals, $f_x^{\text{even}}\approx f_x^{\text{odd}}\approx\frac{1}{2}f_x(0)$, $f_x(L)\to 0$, and $D_z(L)\to 0$. Approximating $\bar{\epsilon}_t(q)$ in Eq. (A10) by the bulk dielectric constant ϵ_t of the metal, one obtains[7]

$$Q_0=f_x(0)=-\frac{k_t}{q_x\epsilon_t}+\frac{2}{i\pi}\int_0^\infty dk\frac{q_x}{q^2}\left[\frac{1}{\bar{\epsilon}_l(\mathbf{q})}-\frac{1}{\epsilon_t}\right]\ , \tag{A25}$$

where $(q_x,0,k_t)$ is the wave vector of the transverse wave in the metallic halfspace, $q_x^2+k_t^2=\epsilon_t\omega^2/c^2$. If we omit the small second term on the right-hand side of Eq. (A25), we obtain from Eq. (A16) the classical Fresnel result for the reflection amplitude. The correction term to the Fresnel result is important for the interpretation of reflection spectroscopy experiments.[1,3,17] However, in the prefactor of the longitudinal field, Eq. (2.10), this term can be neglected.

Whereas the $E_x(z)$ field in a very thin slab is practically constant, the E_z field has an interesting z dependence. To lowest order in $\omega L/c$, only odd values of kL/π contribute to $E_z(z)$ [cf. Eqs. (A9), (A10), and (A22)], and the contributions containing $\bar{\epsilon}_t(q)$ can be neglected,

$$E_z(z)=D_z(0)\left[1+\frac{4}{L}\sum_{\substack{k>0\\ \text{odd}}}\frac{\sin(kz)}{k}\left[\frac{1}{\bar{\epsilon}_l(k)}-1\right]+O(q_xL)\right]\ . \tag{A26}$$

With $\bar{\epsilon}_l(k)\to 1$ for $k\to\infty$, we obtain

$$E_z(0^+)=D_z(0)=\epsilon_a(1+r)E_z^{\text{inc}}(0^-)\ ,$$

where Eq. (A2b) and the matching condition D_z continuous is taken into account and r is given in Eqs. (A16) and (A23). For $\epsilon_a=1$, one recovers Eq. (2.10). For the semi-infinite system, on the other hand, one obtains with the approximation $\bar{\epsilon}_t(\mathbf{q})=\epsilon_t$ from Eqs. (A9) and (A10)

$$\begin{aligned}E_z(z)=D_z(0)\Bigg[&\frac{1}{\epsilon_t}e^{ik_tz}+\frac{2}{\pi}\int_0^\infty dk\frac{k\sin(kz)}{q_x^2+k^2}\\&\times\left[\frac{1}{\bar{\epsilon}_l(\mathbf{q})}-\frac{1}{\epsilon_t}\right]\Bigg]\ ,\end{aligned} \tag{A27}$$

in agreement with Ref. 7. The z dependence of E_z near the surface is in agreement with Eq. (2.9).

In order to calculate the important contribution of the longitudinal fields to the power absorption, it is convenient to treat the transverse fields within the approximation $\bar{\epsilon}_t(\mathbf{q})=\bar{\epsilon}_l(0)\equiv\epsilon_t$, with a "bulk" dielectric constant ϵ_t independent of $\mathbf{q}$. Then Eqs. (A9) and (A10) are evaluated to yield $\mathbf{E}=\mathbf{E}^t+\mathbf{E}^l$, where $\mathbf{E}^t=\mathbf{D}/\epsilon_t$ with

$$D_\mu(z)=\tilde{g}_\mu(z)D_z(0)+\eta_\mu\tilde{g}_\mu(L-z)D_z(L)\ , \tag{A28}$$

$$\tilde{g}_x(z)=-i(k_t/q_x)\cos[k_t(L-z)]/\sin(k_tL)\ , \tag{A29a}$$

$$\tilde{g}_z(z)=\sin[k_t(L-z)]/\sin(k_tL)\ , \tag{A29b}$$

and

$$\begin{aligned}E_\mu^l(z)=-\frac{i}{L}\sum_k\frac{q_\mu}{q^2}&\left[\frac{1}{\bar{\epsilon}_l(\mathbf{q})}-\frac{1}{\epsilon_t}\right]\\&\times[e^{ikz}D_z(0)+\eta_\mu e^{ik(L-z)}D_z(L)]\ .\end{aligned} \tag{A30}$$

Using $\mathbf{j}=i\omega(\mathbf{E}-\mathbf{D})/4\pi$, we can separate the total power absorption

$$P=\tfrac{1}{2}\int_0^L dz\ \mathrm{Re}[\mathbf{j}(z)\cdot\mathbf{E}^*(z)]=P^t+P^l \tag{A31}$$

into contribution

$$P^t=\frac{\omega}{8\pi}\mathrm{Im}\left[-\frac{1}{\epsilon_t}\right]\int_0^L dz\,|\,\mathbf{D}(z)\,|^2 \tag{A32}$$

due to the transverse field and a contribution

$$P^l=-\frac{\omega}{8\pi}\int_0^L dz\,\mathrm{Im}[\mathbf{D}^*(z)\cdot\mathbf{E}^l(z)] \tag{A33}$$

containing the longitudinal field. In Eq. (A33) we may neglect the small x component of $\mathbf{E}^l$ and the z dependence of D_z to obtain for the power absorption related to the longitudinal field at the surface which is exposed to the incident light

$$P^l=-\frac{\omega}{8\pi}\,|\,D_z(0)\,|^2\frac{4}{L}\sum_{\substack{k>0\\ \text{odd}}}\frac{1}{k^2}\mathrm{Im}\left[\frac{1}{\bar{\epsilon}_l(k)}-\frac{1}{\epsilon_t}\right]. \tag{A34}$$

Dividing (for $\epsilon_a=\epsilon_b=1$, $\alpha=\phi$) by the incident flux $c\cos\phi\,|\,E_a\,|^2/8\pi$ and inserting $D_z(0)=\sin\phi E_0(1+r)$ we recover Eq. (2.13) augmented by the term $-1/\epsilon_t$ in the large parentheses, which removes the long-wavelength singularity of Eq. (2.13). Since P^t, Eq. (A32), also remains finite in the limit $L\to\infty$ (there the z dependence of D_z can, of course, not be neglected), the somewhat arbitrary separation of P into P^t and P^l is advantageous.

[1]For a review, see F. Forstmann and R. R. Gerhardts, in *Festkörperprobleme (Advances in Solid State Physics)*, edited by J. Treusch (Vieweg, Braunschweig, 1982), Vol. XXII, pp. 291–323; *Springer Tracts in Modern Physics*, edited by G. Höhler (Springer, Berlin, 1986), Vol. 109, pp. 1–132.

[2]P. J. Feibelman, Phys. Rev. B **12**, 1319 (1975).

[3]P. J. Feibelman, Prog. Surf. Sci. **12**, 287 (1982).

[4]T. Maniv and H. Metiu, Phys. Rev. B **22**, 4731 (1980).

[5]T. Maniv and H. Metiu, J. Chem. Phys. **76**, 696 (1982).

[6]T. Maniv and H. Metiu, J. Chem. Phys. **76**, 2697 (1982).

[7]R. R. Gerhardts and K. Kempa, Phys. Rev. B **30**, 5704 (1984).

[8]N. D. Lang and W. Kohn, Phys. Rev. B **1**, 4555 (1970).

[9]G. E. Korzeniewski, T. Maniv, and H. Metiu, J. Chem. Phys. **76**, 1564 (1982).

[10]D. M. Newns, Phys. Rev. B **1**, 3304 (1970).

[11]P. Gies and R. R. Gerhardts, Phys. Rev. B **31**, 6843 (1985); **33**, 982 (1986).

[12]A. G. Eguiluz, D. A. Campbell, A. A. Maradudin, and R. F. Wallis, Phys. Rev. B **30**, 5449 (1984).

[13]A. G. Eguiluz, Phys. Rev. B **31**, 3303 (1985).

[14]A. Liebsch, Europhys. Lett. **1**, 361 (1986).

[15]W. Ekardt, Z. Penzar, and M. Sunjić, Phys. Rev. B **33**, 3702 (1986).

[16]On the right-hand side of the equation a factor of 2 has been included, which is missing in Ref. 5 due to a typographical error.

[17]K. Kempa and R. R. Gerhardts, Surf. Sci. **150**, 157 (1985).

[18]C. Schwartz and W. L. Schaich, Phys. Rev. B **30**, 1059 (1984).

[19]P. Gies and R. R. Gerhardts, Europhys. Lett. **1**, 513 (1986).

[20]P. J. Feibelman, Phys. Rev. B **23**, 2629 (1981).

[21]K. Kempa and F. Forstmann, Surf. Sci. **129**, 516 (1983).

[22]K. Kempa and R. R. Gerhardts, Solid State Commun. **53**, 579 (1985).

[23]H. J. Levinson, E. W. Plummer, and P. J. Feibelman, Phys. Rev. Lett. **43**, 952 (1979).

[24]A. Bagchi, Phys. Rev. B **15**, 3060 (1977).